Planetary Defense Conference 2013

IAA-PDC13-04-16

Trajectory and Mission Design for the Origins Spectral Interpretation Resource Identification Security Regolith Explorer (OSIRIS-REx) Asteroid Sample Return Mission

Mark Beckman[a,1], Brent W. Barbee[a,2,*], Bobby G. Williams[b,3], Ken Williams[b,4], Brian Sutter[c,5], Kevin Berry[a,2]

[a]*NASA/GSFC, Code 595, 8800 Greenbelt Road, Greenbelt, MD, 20771, USA*
[b]*KinetX Aerospace, Inc., 21 W. Easy St., Suite 108, Simi Valley, CA 93065, USA*
[c]*Lockheed Martin Space Systems Company, PO Box 179, Denver CO, 80201, MS S8110, USA*

Abstract

The Origins Spectral Interpretation Resource Identification Security Regolith Explorer (OSIRIS-REx) mission is a NASA New Frontiers mission launching in 2016 to rendezvous with near-Earth asteroid (NEA) 101955 (1999 RQ_{36}) in 2018, study it, and return a pristine carbonaceous regolith sample in 2023. This mission to 1999 RQ_{36} is motivated by the fact that it is one of the most hazardous NEAs currently known in terms of Earth collision probability, and it is also an attractive science target because it is a primitive solar system body and relatively accessible in terms of spacecraft propellant requirements. In this paper we present an overview of the design of the OSIRIS-REx mission with an emphasis on trajectory design and optimization for rendezvous with the asteroid and return to Earth following regolith sample collection. Current results from the OSIRIS-REx Flight Dynamics Team are presented for optimized primary and backup mission launch windows.

Keywords: interplanetary trajectory, trajectory optimization, gravity assist, mission design, sample return, asteroid

1. Introduction

The Origins Spectral Interpretation Resource Identification Security Regolith Explorer (OSIRIS-REx) mission is a NASA New Frontiers mission launching in 2016. It will rendezvous with near-Earth asteroid (NEA) 101955 (1999 RQ_{36}) in 2018, study and map the NEA, determine the effect of the Yarkovsky force on its heliocentric orbit, and return a pristine carbonaceous regolith sample in 2023. (101955) 1999 RQ_{36} is an approximately 550-m diameter NEA and is one of the most potentially hazardous of all the currently known potentially hazardous asteroids (PHAs), based on its size and probability of future impacts with Earth. Ways in which the OSIRIS-REx mission helps inform and enable future planetary defense missions are detailed in in Ref. 1. 1999 RQ_{36} is also a member of the rare B-type subgroup of the carbonaceous C-type asteroids. Its primitive nature (here meaning relatively unprocessed since formation) makes it an attractive science target. Its relatively low-inclination, Earth-like orbit makes it accessible in terms of spacecraft Δv requirements.

OSIRIS-REx will be only the third mission ever to visit a NEA, following the NEAR-Shoemaker mission to 433 Eros and the JAXA Hayabusa mission to 25143 Itokawa. It presents a variety of flight dynamics and mission design challenges, such as designing safe and effective captured orbits and other ballistic proximity operations trajectory sequences about the NEA for surface mapping activities. It is especially challenging in the area of

*Corresponding author

Email addresses: mark.beckman@nasa.gov (Mark Beckman), brent.w.barbee@nasa.gov (Brent W. Barbee), bobby.williams@kinetx.com (Bobby G. Williams), kenneth.williams@kinetx.com (Ken Williams), brian.mspc.sutter@lmco.com (Brian Sutter), kevin.e.berry@nasa.gov (Kevin Berry)

[1]Flight Dynamics System Manager for OSIRIS-REx Mission
[2]Aerospace Engineer, Navigation and Mission Design Branch
[3]Director of Space Navigation and Flight Dynamics (SNAFD)
[4]Navigation Team Chief for OSIRIS-REx Mission
[5]Mission Design Lead for OSIRIS-REx

designing combined ground-based and onboard guidance algorithms to execute the demanding Touch and Go (TAG) maneuver sequence for regolith sample collection using onboard ephemeris knowledge, optical navigation, and laser ranging. The OSIRIS-REx Flight Dynamics System (FDS) team has developed a number of innovative techniques for addressing these design issues. Other challenging aspects of the overall mission design include optimization of the outbound cruise trajectory, which includes an Earth gravity assist bracketed by optimized Deep Space Maneuvers (DSMs). The asteroid approach phase at the end of outbound cruise culminates in a specially designed set of asteroid approach maneuvers to ensure a safe rendezvous as the mission team uses the spacecraft cameras to search for and acquire the NEA, ascertain whether any natural satellites are present in the vicinity of the NEA, and perform initial mass determination for the NEA.

In this paper we provide an overview of the current mission design results with a focus on the design and optimization of the trajectories required to rendezvous with RQ_{36} for sample collection and later return to Earth with the pristine regolith sample. In particular, we present some of the most recent results produced by the OSIRIS-REx FDS team in terms of optimized trajectories for the mission launch windows for outbound cruise to the asteroid.

2. Destination: Near-Earth Asteroid 101955 (1999 RQ_{36})

The destination of the OSIRIS-REx mission is the NEA 101955 (1999 RQ_{36}), referred to herein as 1999 RQ_{36} or simply RQ_{36}. This NEA is one of 1381 currently known Potentially Hazardous Asteroids (PHAs)[6] because its Minimum Orbit Intersection Distance (MOID) with Earth's orbit of 0.00296049 AU is ≤ 0.05 AU and its absolute magnitude, H, of 20.812 is ≤ 22.0. Based on current modeling and knowledge of the orbit of RQ_{36}, there are eight potential collisions with Earth between the years 2169 and 2199, with a cumulative impact probability of 7.1×10^{-4}. At an approximate diameter of 550 m, this NEA would deliver approximately 2700 MT of energy should it impact the Earth. A simulated image[7] of RQ_{36} is presented in Figure 1.

Figure 1: Simulated image of 1999 RQ_{36} - topography overlaid on radar imagery (Credit: NASA/GSFC/UA).

In addition to being one of the most hazardous NEAs currently known, RQ_{36} is also among the best characterized due to the significant number of optical and radar observations that have been collected since its discovery in 1999. These observations have led to estimates of the NEA's rotational period (4.2978 hours), and we have been able to see that its rotation is retrograde with an obliquity of $174^\circ \pm 10^\circ$. At this time no non-principal axis rotation has been detected. Radar-derived shape models and constraints on the bulk density have led to the following range of values, in units of km^3/s^2, for the NEA's gravitational parameter, μ: 2.93×10^{-9} (low), 4.16×10^{-9} (nominal), and 6.6249×10^{-9} (high).

[6] `http://neo.jpl.nasa.gov/neo/groups.html`, accessed on 2013-03-07

[7] See `http://osiris-rex.lpl.arizona.edu/?q=gallery`, accessed on 2013-03-07.

The heliocentric classical Keplerian orbital elements of the orbit of RQ_{36}[8] are presented in Table 1 for reference. As mentioned previously, this NEA's orbit semi-major axis is near 1 AU, and both its orbital eccentricity and inclination are relatively low. Those features of its orbit make it relatively accessible for rendezvous in terms of required mission Δv.

Table 1: Heliocentric ecliptic J2000 orbital elements for 1999 RQ_{36} at epoch JD 2456400.5 (2013-04-18.0) TDB (JPL Orbit ID 64).

Orbital Element	Value
Semi-major axis, a (AU)	1.12600
Eccentricity, e	0.20373
Inclination, i	6.03491°
Longitude of Ascending Node, Ω	2.04227°
Argument of Perihelion, ω	66.2686°
Mean Anomaly at Epoch, M	72.8280°

3. Mission Design Overview

In this section we provide an overview of the OSIRIS-REx mission design. The OSIRIS-REx spacecraft design draws upon heritage from the MAVEN spacecraft[9] and the Sample Return Capsule (SRC) draws upon heritage from the Stardust[10] SRC. Accordingly, the SRC will be delivered to a direct atmospheric entry upon return to Earth at the conclusion of the mission.

The total duration of the round-trip mission is seven years, consisting of a 2 year outbound cruise from Earth to the NEA, 2.5 years at the NEA (during which observations and sampling are performed), and a 2.5 year return cruise to bring the collected sample to Earth. All of the observation and sampling activities at the NEA are scheduled to be accomplished during the first half of the 2.5 years at the NEA, leaving the remaining half of that time as available schedule reserve for contingencies. Two years of sample curation and analysis follow sample return.

3.1. Outbound Cruise and Approach Phase

The primary launch window is required to span at least 21 days, but we are able to construct a 39 day window, as will be detailed subsequently. Each day in the launch window has a 30 minute daily launch window, with launch times during the early evening. The Earth departure characteristic energy, C_3, is held constant across the primary launch window at 29.3 km^2/s^2, by design, and the assumed spacecraft wet mass is 1955 kg based on a notional launch vehicle capability. Current propulsion system assumptions are a monopropellant system with a specific impulse of 230.7 seconds and a pulse mode specific impulse of 170 seconds. The main thrust level is assumed to be 661 N. During launch, the hyperbolic injection will occur approximately 10 minutes prior to achieving acquisition of signal (AOS) with the Deep Space Network (DSN), and spacecraft separation from the launch vehicle occurs 3 minutes thereafter.

Trajectories launching during the primary launch window in September-October of 2016 involve a 1 year Earth-to-Earth trajectory that includes one DSM and during which the minimum distance to the Sun is 0.78 AU. The Earth-to-Earth trajectory culminates in an Earth Gravity Assist (EGA) for which the perigee altitude is between 17,100 and 27,000 km. The EGA rotates the spacecraft trajectory into the RQ_{36} orbit plane, after which the spacecraft spends another year traveling to the asteroid. An additional DSM is performed between EGA and asteroid arrival. The spacecraft will be between approximately 0.8 and 1.4 AU from the Sun for the majority of the mission.

The asteroid approach phase is divided into 3 deterministic Asteroid Approach Maneuvers, 14 days apart, labeled AAM1, AAM2, AAM3. Optical navigation observations begin 47 days before AAM1 (although the camera requires acquisition only 21 days before AAM1). During approach a survey of the asteroid's vicinity will be performed to search for any natural satellites (10 cm in size or larger) that may be present. The solar phase angle relative to the asteroid is $< 50°$ during the natural satellite survey to ensure sufficient lighting for visibility.

[8] See `http://ssd.jpl.nasa.gov/sbdb.cgi?sstr=1999RQ36`, accessed on 2013-03-07.

[9] The Mars Atmosphere and Volatile EvolutioN (MAVEN) mission is scheduled to launch in November of 2013 and will study the Martian atmosphere and better understand Mars climate evolution and loss of atmosphere (and water) over time.

[10] Stardust was a robotic spacecraft mission launched in 1999 to collect dust samples from the coma of Wild 2 and return them to Earth. It was the first mission of its kind and its SRC set a record spacecraft atmospheric entry speed of 12.9 km/s.

3.2. Preliminary and Detailed Survey Phases

After approach the preliminary survey phase begins, during which the spacecraft will perform 3 flybys of the asteroid with a closest approach distance of about 7 km. One flyby will be over the north pole, one will be over the south pole, and the other will be over the equator. The spacecraft speed relative to the asteroid during these flybys will be about 20 cm/s.

Following preliminary survey is the detailed survey phase, during which the spacecraft will collect observations of the asteroid from specific solar phase angle stations. The spacecraft will take two days to travel from south to north for each station, and observations are collected for 4.5 hours during the equatorial crossing of each station (recall that the asteroid rotates once every 4.3 hours). Safe mode entry would not require active maneuvers to avoid contact with the asteroid throughout the survey phase.

During the flybys and subsequent close approaches to RQ_{36}, the spacecraft tracking data are used to estimate improved values for the physical characteristics of the asteroid that affect details of the subsequent proximity orbit design. This includes estimates of the spin state, gravitational parameter, and gravity field harmonic coefficients of RQ_{36}.

3.3. Orbital Phase

The next phase is referred to as the orbital phase, and it is during this phase that the spacecraft enters into a captured orbit about the asteroid (bound by the asteroid's gravity). The orbit radius will be between 1.0 and 1.5 km during the orbital phase and the orbits are designed such that no orbit maintenance maneuvers are required for at least 21 days. For stability relative to solar pressure, these orbits are designed to reside in the terminator plane.

The spacecraft resides in Orbit A from December 31st, 2018 until January 20th, 2019. The nominal orbit radius is 1.5 km and therefore has an approximately 50 hour orbit period and a 5.3 cm/s orbital velocity. The spacecraft transfers to Orbit B on January 21st, 2019 and remains in this orbit until March 5th, 2019. Orbit B has a nominal radius of 1 km, a 27 hour orbit period, and a 6.5 cm/s orbital velocity. Note that orbit periods and velocities stated here assume the aforementioned nominal value of the asteroid gravitational parameter.

3.4. Recon Phase

After the orbital phase is complete, a set of candidate sampling sites on the asteroid's surface will have been selected. The next phase is the recon phase, the purpose of which is to obtain more detailed observations of the candidate sampling sites. Four close observations will be performed at a flyby range of 225 m to verify the presence of material that the spacecraft's sampling head can ingest. To perform the recon flybys, the spacecraft will leave the aforementioned terminator plane orbit at the equatorial crossing and fly in a prograde sense across the sunlit side of the asteroid. Candidate sampling sites will be observed at 30° phase angle (higher latitudes will have higher angles). The spacecraft then recaptures into the terminator plane orbit 5 hours after it departed. There are then two weeks of orbital operations before the next 225 m recon flyby during which maneuvers are designed and phasing maneuvers are performed. After the four 225 m recon flybys are completed there will be one 500 m recon flyby to obtain spectrometer data over the expected sampling region. The rehearsals for sample collection begin two weeks after the 500 m recon flyby is completed.

3.5. TAG Rehearsals and TAG

Three TAG rehearsal trajectories are flown to verify the ability to target the TAG site within requirements. The TAG rehearsal maneuvers follow a similar structure to the actual TAG maneuvers, beginning with a phasing maneuver about 7 days prior to the nominal TAG time. The phasing maneuver leads to the spacecraft being at the proper point in the orbit at the proper time to descend to the desired point on the asteroid's surface, accounting for the asteroid's rotational state. The orbit departure maneuver places the spacecraft on a prograde trajectory that brings it to a point 125 m above the TAG site, referred to as the checkpoint. The orbit departure latitude is opposite the TAG site latitude, and approximately 4 hours of flight time elapse between orbit departure and arrival at checkpoint.

The maneuver performed at checkpoint places the spacecraft onto a trajectory that intersects the asteroid, with a 16 cm/s approach velocity. Approximately 600 seconds later the spacecraft arrives at the matchpoint location 45 m above the asteroid's surface, where a final maneuver is performed to adjust the approach velocity down to 10 cm/s. After the spacecraft sampling system has contacted the asteroid's surface and ingested the regolith sample, a 0.5 m/s escape maneuver is performed to move the spacecraft up and away from the asteroid. The mission Δv budget has 1.61 m/s included three times to allow all three TAG rehearsals to be repeated three times. Moreover, the mission Δv budget includes one entire asteroid proximity operations sequence (22 m/s) as unallocated margin. It is important to note that the Δv budget includes allocations for three complete TAG attempts, including three rehearsals for each of those three attempts. The proximity operations sequence includes the approach, survey, orbital, and recon phases described previously. Detailed development and discussion of the TAG guidance algorithms and expected performance under various conditions is provided in Ref. 2

3.6. Asteroid Departure and Earth Return

The spacecraft will nominally depart the asteroid on March 3rd, 2021 and return to Earth 935 days later on September 24th, 2023 with an atmospheric entry speed of 12.198 km/s, which is within the OSIRIS-REx limit of 12.4 km/s. Alternatives to this baseline asteroid departure and Earth return scenario are elaborated on in a subsequent section. The asteroid departure maneuver initially targets an Earth flyby at a distance of at least 10,000 km from Earth, and a series of planned "walk-in" maneuvers will be used to gradually lower the perigee altitude, as was done for the Stardust mission. After the appropriate atmospheric entry interface has been successfully targeted, the SRC will separate from the spacecraft and continue to Earth while the spacecraft performs a maneuver to raise perigee well above an entry condition and proceed to follow a solar orbit that remains clear of the celestial bodies in our solar system as per Planetary Protection requirements.

3.7. Mission Δv Budget

An example mission Δv budget corresponding to the worst (highest total post-launch Δv) day of the primary launch window is presented in Table 2[11]. It is worth noting that even on the worst day of the launch window we have 73 m/s of unallocated Δv, which is 117% of the 62 m/s allocated to the statistical Trajectory Correction Maneuver (TCM) budget. As mentioned previously, the Δv budget also includes 100% unallocated margin for proximity operations Δv (22 m/s). Furthermore, the spacecraft propellant tank is sized to convert all unused dry mass margin into propellant. These aspects of the mission and spacecraft design provide the OSIRIS-REx mission with a robust Δv budget.

Table 2: Example OSIRIS-REx mission Δv budget assuming launch on the most demanding day of the primary launch window.

Maneuver/Event	Pre-Event Mass (kg)	Main Δv (m/s)	Monoprop Mass (kg)	Pulse Mode Δv (m/s)	Pulse Prop Mass (kg)	Post-Event Mass (kg)
Post Launch - Initial Acquisition	1955.0	0.0	0.0	1.0	1.4	1953.6
Post Launch TCMs	1953.6	52.0	44.4			1909.3
DSM1	1909.3	472.6	359.9			1549.3
Outbound Cruise ACS Desat	1549.3				4.0	1545.3
DSM2	1545.3	49.0	33.1			1512.2
AAM1	1512.2	375.8	231.5			1280.7
AAM2	1280.7	150.9	82.6			1198.1
AAM3	1198.1	4.7	2.5			1195.6
Preliminary Survey	1195.6			1.3	1.1	1194.5
Detailed Survey	1194.5			1.3	1.0	1193.5
Orbit Operations	1193.5			0.1	0.1	1193.4
Surface Reconnaissance	1193.4			1.0	0.8	1192.6
Sampling Rehearsals	1192.6			1.6	1.3	1191.2
Sampling Operations	1191.2			1.2	1.0	1190.3
Δv to Repeat Rehearsals and Sampling Twice	1190.3			5.6	4.6	1185.7
10 Orbit Departures and Recaptures	1185.7			10.0	8.2	1177.5
Proximity Operations ACS Desat	1177.5				4.2	1173.3
1999 RQ_{36} Departure & Earth Targeting	1173.3	320.1	154.8			1018.5
Inbound Cruise TCMs	1018.5	10.0	5.2			1013.3
Earth Return Cruise ACS Desat	1013.3				4.6	1008.7
Deflection from Earth (after sep of 50 kg SRC)	958.7	17.5	7.4			951.4
Unallocated Δv Margin	951.4	73.0	30.2	22.0	13.9	907.2
Final Totals	891.9	1525.6	951.6	45.0	46.2	

4. Trajectory Design Overview

The interplanetary trajectories flown by the OSIRIS-REx mission incorporate several key advanced trajectory design elements including optimally located and oriented Deep Space Maneuvers (DSMs), multiple revolutions about the Sun, and an Earth Gravity Assist (EGA). Those elements are able to reduce mission Δv requirements at the expense of requiring more challenging calculations and lengthening flight times. Herein we motivate and describe this trade-off for the OSIRIS-REx mission and provide a detailed description of the mission trajectory design.

[11] The mass evolution in Table 2 accounts for 11.5 kg of unusable propellant and 3.8 kg of Helium pressurant.

4.1. Preliminary Trajectory Analysis

The benefits and costs of utilizing the aforementioned advanced trajectory design techniques are well illustrated by beginning with a simpler trajectory design against which the more advanced design is compared. One common technique for identifying optimal departure dates for missions is to perform broad trajectory grid scans using straightforward Lambert targeting to produce ballistic trajectory segments to the destination with no DSMs or gravity assists. Lambert targeting algorithms that support multiple revolutions about the central body are available but are generally more challenging to utilize than targeters that are restricted to producing trajectories that make at most just slightly less than one full revolution between departure and arrival (i.e., transfer angle $< 2\pi$), referred to as "Type II" Lambert trajectories.

We perform two Lambert targeting grid scans, one for outbound trajectories from Earth to the asteroid, and a second scan for inbound trajectories from the asteroid back to Earth. We exploit some insight here in the selection of the range of departure dates scanned in that we recognize that the minimum Δv solution will likely require a total round-trip flight time on the order of the synodic period between the asteroid and Earth, which is approximately 6 years; this clearly necessitates a long stay time at the asteroid, but that is desirable for OSIRIS-REx mission operations. Pork Chop Contour (PCC) plots for these two trajectory scans are presented in Figure 2.

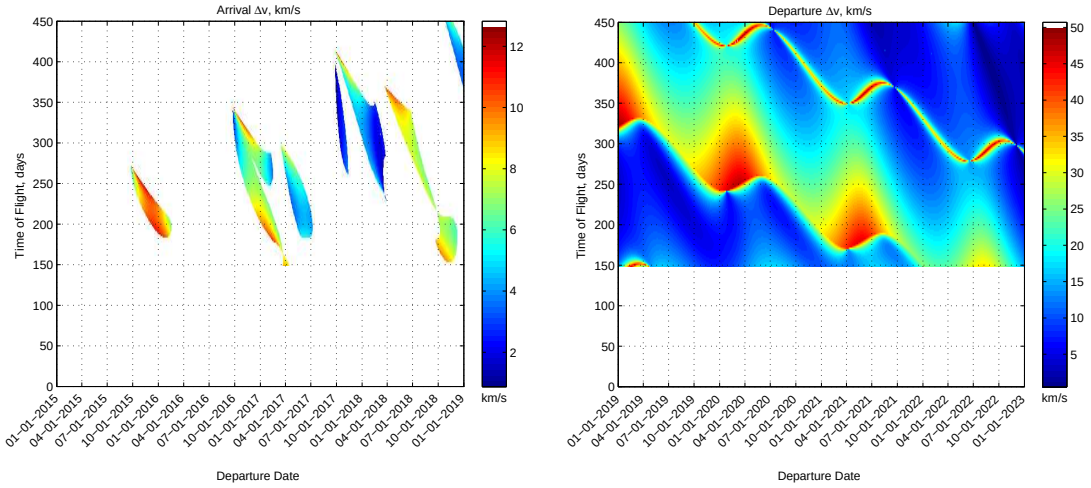

(a) PCC plot of Δv to arrive at RQ_{36}.

(b) PCC plot of Δv to depart from RQ_{36}.

Figure 2: PCC plots showing Δv required to arrive at and depart from RQ_{36} as a function of departure date and flight time.

The arrival Δv scan visualized in Figure 2(a) is constrained to have Earth departure characteristic energy, C_3, ≤ 29.3 km^2/s^2 and Earth departure Declination of the Launch Asymptote (DLA) bounded by $\pm$ 36°. Those constraints clearly restrict the available solutions, and there is a distinct minimum in arrival Δv right around October 1st, 2017 with a flight time to the asteroid between 300 and 400 days. Figure 2(b) shows a minimum for the Δv needed to depart the asteroid at an asteroid departure date somewhere between July and October of 2022, with a flight time to return to Earth of between 350 and 450 days. The absolute minimum arrival and departure Δv solutions were recorded by the trajectory scan algorithm and the overall round-trip trajectory solution they comprise is presented in the first column of data (under the heading "Type II Lambert") in Table 3.

The key finding from these trajectory scan results is that late September of 2017 is an optimal time to depart Earth for rendezvous with RQ_{36} because at that time Earth happens to be near the line of intersection between its orbit plane and that of RQ_{36}, which allows the launch vehicle to place the spacecraft in very nearly the correct plane and thus minimize post-launch Δv burden. Table 3 presents results for the Lambert scans and for the more advanced OSIRIS-REx trajectory designs in terms of the best and worst days of both the primary and backup launch windows, which will be discussed in detail in subsequent sections. For now it is important to note the benefits and costs of the multi-revolution trajectory solutions that leverage optimized DSMs and, in the case of the primary launch window, an EGA. The OSIRIS-REx mission requires at least 435 days to be spent in proximity of the asteroid for data and sample collection activities, and all of the trajectory solutions in Table 3 provide more than enough stay time at the asteroid. However, the advanced trajectory solutions of the primary and backup launch windows trade some time at the asteroid for the benefit of reducing the mission Δv compared to the Type II Lambert solution. Furthermore, those trajectory types achieve a much more favorable atmospheric entry speed

Table 3: Comparison of trajectory design types for the OSIRIS-REx mission.

		Primary LW (DSMs, multi-rev, EGA)		Backup LW (DSM, multi-rev)	
	Type II Lambert	Best	Worst	Best	Worst
Earth Departure Date	09/27/2017	09/19/2016	09/04/2016	09/25/2017	10/05/2017
Earth Departure DLA	33.36°	0.11°	2.13°	33.09°	33.25°
Earth Departure C_3 (km^2/s^2)	29.0	29.3	29.3	29.1	29.0
Flight Time to RQ_{36} (days)	382	784	799	413	403
NEA Arrival Date	10/14/2018	11/12/2018	11/12/2018	11/12/2018	11/12/2018
Total Post-launch Δv to Arrive at RQ_{36} (m/s)	874	831	1058	670	1123
Stay Time at RQ_{36} (days)	1387	842	842	842	842
RQ_{36} Departure Date	08/01/2022	03/03/2021	03/03/2021	03/03/2021	03/03/2021
RQ_{36} Departure Δv (m/s)	494	320	320	320	320
Flight Time to Earth (days)	422	935	935	935	935
Earth Arrival Date	09/27/2023	09/24/2023	09/24/2023	09/24/2023	09/24/2023
Atmospheric Entry Speed (km/s)	12.88	12.20	12.20	12.20	12.20
Total Post-launch Round-Trip Δv (m/s)	1368	1151	1378	990	1443
Total Round-Trip Mission Duration (years)	6.00	7.01	7.05	6.00	5.97

at Earth return. All that being said, the straightforward Type II Lambert approach yields a total mission Δv that is a reasonable predictor of the amount of Δv required by the more advanced methods when considering the spread between the best and worst days of the launch windows.

4.2. Overview of the Outbound Trajectory Designs

As noted previously, the most advantageous time for departing Earth to rendezvous with RQ_{36}, in terms of minimizing the required Δv, occurs in September of 2017 when Earth is near the line of intersection between its orbit plane and that of RQ_{36}. This geometry permits the launch vehicle to insert OSIRIS-REx into an outbound trajectory that begins essentially coplanar with the asteroid's heliocentric orbit. However, further analysis has demonstrated that achieving this geometry in 2017 is possible by launching approximately one year earlier, in September of 2016, and performing an Earth Gravity Assist (EGA) in 2017 to place OSIRIS-REx in the RQ_{36} orbit plane. The total post-launch Δv costs are similar for these two options (2016 launch and 2017 launch), although the 2016 opportunity offers several advantages that will be discussed in detail. First, it supports a launch window that is nearly twice as large as the 2017 launch window. Second, it offers Declination of the Launch Asymptote (DLA) values that are well within the range of ± 28.5°, for which most launch vehicles provide their best performance. Third, the characteristic Earth departure energy, C_3, can be kept constant across the 2016 launch window, which helps to standardize the spacecraft design and simplify the targeting interface with the launch vehicle provider because there is no variation in the required departure energy and therefore no variation in the injected mass capability of the launch vehicle across the launch window.

The 2016 launch window was therefore selected as the primary launch window for the OSIRIS-REx mission and consists of 39 days, beginning on September 4th, 2016. The 2017 launch opportunity has been designated as the backup launch window for OSIRIS-REx and consists of 21 days, beginning on September 15th, 2017. Outbound cruise trajectories (traveling from Earth to the asteroid) flown from any day in the primary launch window include a first deterministic DSM, DSM1, between Earth departure and the EGA, and a second deterministic DSM, DSM2, between the EGA and asteroid arrival. This trajectory sequence for the first day of the primary launch window is depicted in Figure 3 from a three-dimensional perspective, while an ecliptic plane projection of the trajectory sequence is shown in Figure 4.

Outbound cruise trajectories flown from any day in the backup launch window involve only one DSM, DSM1, that is executed between Earth departure and asteroid arrival. For primary launch window trajectories, DSM1 targets the appropriate conditions for the EGA, while DSM2 always targets arrival at a location 6300 km from RQ_{36} on October 5th, 2018. For backup launch window trajectories, DSM1 targets the same asteroid arrival conditions that are targeted by DSM2 during primary launch window trajectories. The backup launch window trajectory sequence for the first day of the launch window is visualized in Figure 5 from a three-dimensional perspective, while an ecliptic plane projection of the trajectory sequence is shown in Figure 6.

The asteroid arrival conditions are purposely standardized such that the same arrival sequence is always executed regardless of which launch window, or day within the launch window, is utilized. This is a robust approach because it provides a single set of arrival circumstances for which the spacecraft must be designed, and those circumstances include favorable natural illumination of the asteroid from the spacecraft's vantage point. The Asteroid Arrival Maneuver (AAM) is divided into three parts to create a gentle approach to RQ_{36} that affords adequate time to optically acquire the asteroid using the spacecraft's onboard cameras and also use those cameras to survey the vicinity of the asteroid for any natural satellites that may be present (down to 10 cm in size). Furthermore, the

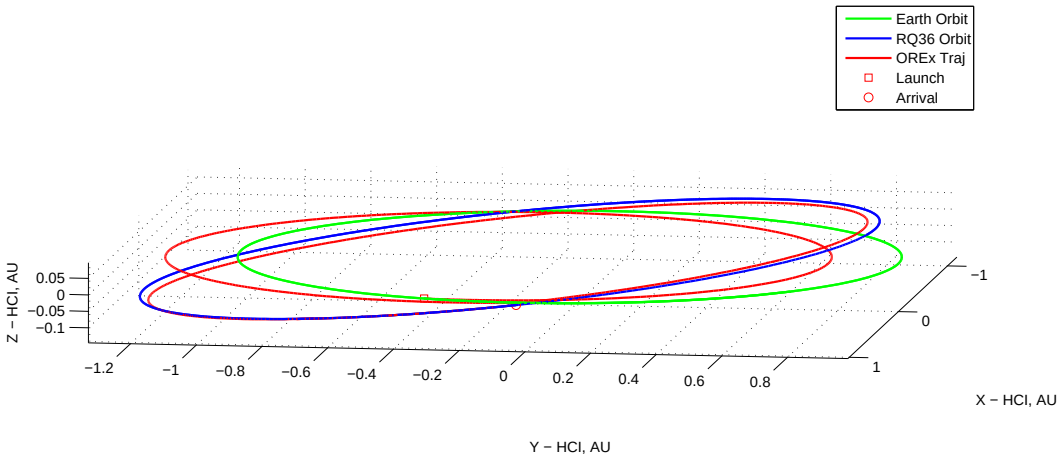

Figure 3: OSIRIS-REx primary launch window outbound cruise trajectory to 1999 RQ_{36}, 3D view.

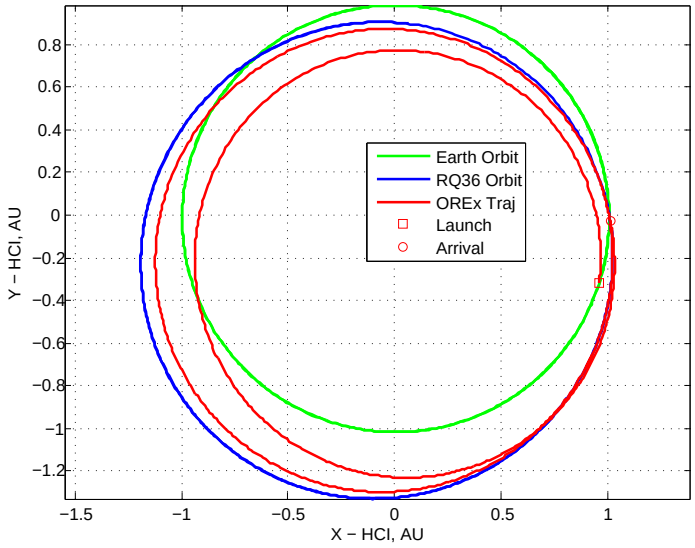

Figure 4: OSIRIS-REx primary launch window outbound cruise trajectory to 1999 RQ_{36}, ecliptic plane projection.

design of the AAM sequence is such that it is possible to gracefully recover if the first maneuver is not executed, which provides additional robustness.

AAM1 is performed on October 1st, 2018 and targets arrival at a location 6300 km from RQ_{36} 14 days later on October 15th, 2018. This is the same point relative to RQ_{36} that is targeted by DSM2. Thus, if AAM1 is not executed, the spacecraft will simply arrive at that location on October 5th, 2018, whereas if AAM1 is executed the spacecraft arrives at that location on October 15th, 2018. AAM2 is nominally performed on October 15th, 2018 and targets arrival at a location 270 km from RQ_{36} 14 days later on October 29th, 2018. Upon arrival at that point, AAM3 is performed, which targets arrival at a location 19.3 km from RQ_{36} 14 days later on November 12th, 2018. Note that if AAM1 is missed as described above, the magnitude of the AAM2 maneuver will be larger because the spacecraft will arrive at the AAM2 point with more relative velocity than it would have otherwise.

The optimal trajectory for each day in the primary launch window is found by holding the day and time of launch constant (for the particular day in the launch window), holding Earth departure C_3 constant, and allowing the following trajectory design parameters to vary: DLA; Right Ascension of the Launch Asymptote (RLA); time, direction, and magnitude of DSM1; time, orientation, and altitude of the EGA flyby; time, direction, and magnitude of DSM2; and the directions and magnitudes of AAM1, AAM2, and AAM3. The goal of the optimization is to minimize the total post-launch Δv needed to arrive at the asteroid, which is given by the sum of the magnitudes of DSM1, DSM2, AAM1, AAM2, and AAM3. The optimization procedure for each day in the backup window is the same, except that there is only one DSM (DSM1) and no EGA.

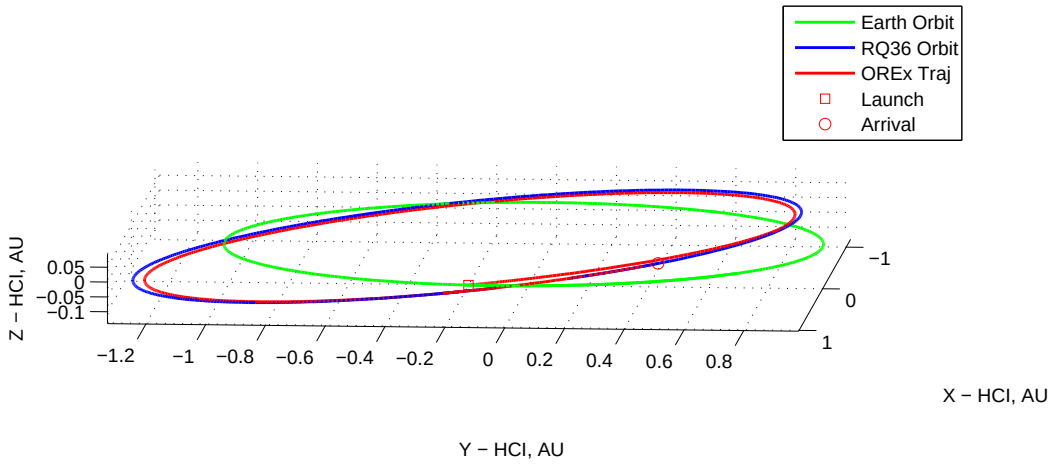

Figure 5: OSIRIS-REx backup launch window outbound cruise trajectory to 1999 RQ_{36}, 3D view.

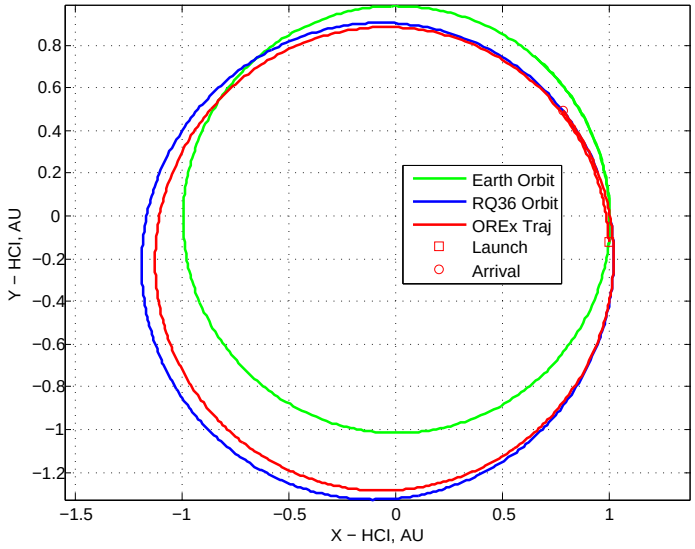

Figure 6: OSIRIS-REx backup launch window outbound cruise trajectory to 1999 RQ_{36}, ecliptic plane projection.

4.3. Overview of the Inbound Trajectory Designs

The fact that the round-trip mission duration is at least one Earth/asteroid synodic period effectively decouples the outbound and inbound trajectories such that they can be optimized independently. This means that the same inbound trajectory may be flown regardless of which launch window (primary or backup) or day of launch window is actually utilized for the outbound flight.

A continuum of asteroid departure opportunities is available and the baseline nominal asteroid departure maneuver occurs on March 3rd, 2021. That departure opportunity requires 316 m/s of Δv and leads to Earth return 935 days later on September 24th, 2023 with an atmospheric entry speed of 12.198 km/s, which is within the OSIRIS-REx limit of 12.4 km/s. The minimum asteroid departure Δv solution is another option within the continuum of departure opportunities. The minimum Δv departure opportunity occurs on May 22nd, 2021 with a Δv of 250 m/s and returns to Earth on September 25th, 2023 with an atmospheric entry speed of 12.390 km/s. The departure window extends to June 28th, 2021, which is the latest possible asteroid departure date that does not exceed the aforementioned nominal asteroid departure Δv. Asteroid departure on June 28th, 2021 requires 313 m/s of Δv and returns the spacecraft to Earth on September 27th, 2023 with an atmospheric entry speed of 12.385 km/s.

There is small chance that the spacecraft could return to Earth one year earlier than planned via a larger asteroid departure maneuver of 935 m/s executed on January 3rd, 2020. This would lead to Earth return on September 24th, 2022 with an atmospheric entry speed of 12.24 km/s. However, this early return option will only be available if a number of criteria are all met. The dry mass of the spacecraft must not grow by more than a very small

amount between now and launch, launch must occur during the middle 21 days of the 39 day primary launch window, AAM1 must occur on or after October 1st, 2018, and science observations and sample collection must be complete within 460 days or less after AAM1. This early departure scenario is merely a possibility that we want to be aware of at this point and is not part of the baseline mission design.

The asteroid departure maneuver initially targets an Earth flyby at a distance of at least 10,000 km from Earth, and a series of planned "walk-in" maneuvers will be used to gradually lower the perigee altitude. This procedure closely follows Stardust mission heritage. The walk-in maneuvers will occur at entry minus 60 days, entry minus 10 days, entry minus 29 hours, and entry minus 12 hours (as a contingency). Altogether, these walk-in maneuvers require approximately 4 m/s of Δv in addition to the asteroid departure maneuver Δv values stated previously. After achieving the appropriate entry trajectory, the Sample Return Capsule (SRC) will separate to continue on the entry trajectory while the OSIRIS-REx spacecraft will perform a 17 m/s Δv to raise its perigee altitude. This satisfies the Planetary Protection requirement that the spacecraft reside in a solar orbit that will not approach any closer than 250 km to the Earth, Moon, or other solar system body. After raising perigee following SRC separation the spacecraft's solar orbit will have a perihelion distance of 0.5 AU, an aphelion distance of 1.0 AU, and a period of 0.66 years.

The entry conditions for the SRC are defined by a 6503.14 km atmospheric entry interface radius, a 12.2 km/s entry speed (nominal), and an inertial entry flight path angle of $-8.2°$. The entry trajectory is targeted to deliver the SRC to the Utah Test and Training Range (UTTR) for retrieval after landing.

5. Trajectory Design and Optimization Results for the Primary and Backup Launch Windows

As described previously, the launch windows are defined by computing the optimal (minimum post-launch Δv) outbound trajectory sequence for each day of the launch window. The optimization is performed by holding the launch day fixed and varying the DLA and RLA, the times, orientations, and magnitudes of DSM1, DSM2, AAM1, AAM2, and AAM3, and the time, orientation, and altitude of the EGA. Recall that for the backup launch window cases there is only one DSM (DSM1) and C_3 is also varied, whereas C_3 is held constant for each day of the primary launch window.

5.1. Primary Launch Window

The variation in DLA for the optimized primary launch window solutions is presented in Figure 7, and these data illustrate one of the advantages of the primary launch window, which is that the DLA is within the range of $-9°$ to $+3°$ throughout the launch window.

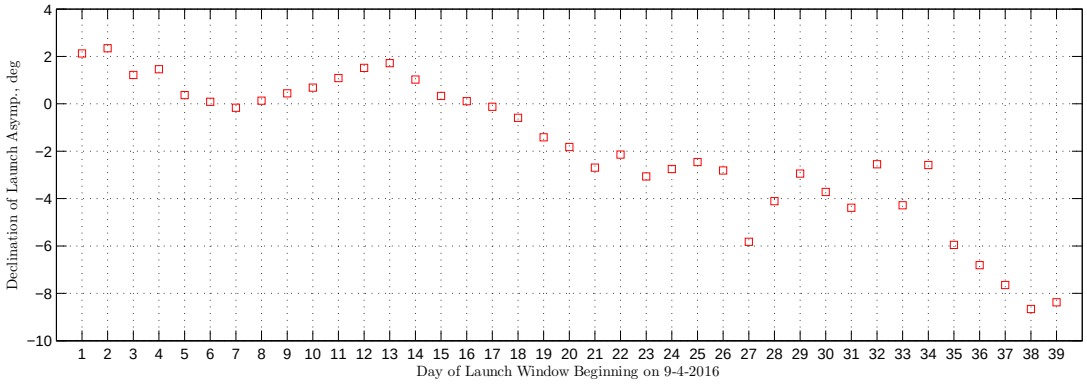

Figure 7: DLA variation throughout the primary launch window.

The total post-launch Δv (for outbound cruise) for each day in the primary launch window is shown in Figure 8. Note that the Δv reaches a minimum on days 16 and 17 of the launch window. The higher Δv at the beginning and end of the 39 day primary launch window are feasible, but the primary launch window could be restricted to the middle 21 days if necessary to reduce Δv requirements. The discontinuity in post-launch Δv between days 26 and 27 is due to a relatively close lunar encounter during Earth departure.

The details of the optimal solutions for each day in the primary launch window are provided in Table 4, including the RLA values and the magnitudes of each individual maneuver. All of the maneuvers except AAM3 vary throughout the launch window in different ways, but the net result is a steady decrease in total Δv until days 16 and 17 and a general increase thereafter through day 39.

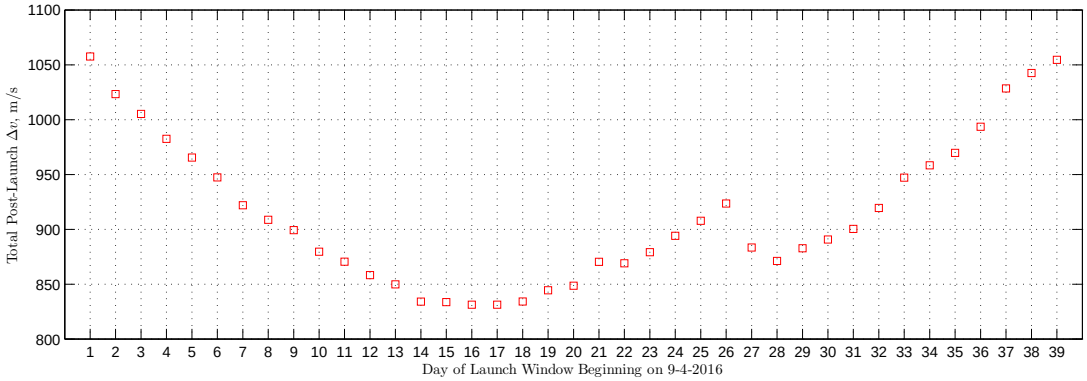

Figure 8: Total Post-Launch Δv variation throughout the primary launch window.

Table 4: Optimized outbound cruise trajectory solutions for each day of the primary launch window.

Day	Date	C_3 (km^2/s^2)	DLA	RLA	DSM1 (m/s)	DSM2 (m/s)	AAM1 (m/s)	AAM2 (m/s)	AAM3 (m/s)	Total Δv (m/s)
1	9-4-2016	29.3	2.13°	173.31°	530.03	7.05	365.80	149.94	4.77	1057.57
2	9-5-2016	29.3	2.34°	174.28°	505.47	1.09	363.19	148.84	4.77	1023.37
3	9-6-2016	29.3	1.22°	174.74°	488.91	0.89	362.17	148.55	4.71	1005.24
4	9-7-2016	29.3	1.46°	175.78°	465.46	0.30	363.19	148.84	4.77	982.56
5	9-8-2016	29.3	0.37°	176.16°	448.16	1.32	362.98	148.30	4.71	965.48
6	9-9-2016	29.3	0.09°	176.93°	425.33	1.86	365.75	149.68	4.77	947.39
7	9-10-2016	29.3	-0.16°	177.66°	406.52	0.93	366.13	143.66	4.71	921.96
8	9-11-2016	29.3	0.13°	178.69°	385.97	13.31	358.00	146.61	4.77	908.65
9	9-12-2016	29.3	0.44°	179.73°	370.80	28.23	351.35	144.15	4.71	899.24
10	9-13-2016	29.3	0.69°	180.76°	356.38	25.04	350.49	142.93	4.71	879.55
11	9-14-2016	29.3	1.09°	181.83°	337.51	30.93	353.39	144.01	4.71	870.55
12	9-15-2016	29.3	1.52°	183.07°	331.28	17.00	359.62	145.62	4.71	858.23
13	9-16-2016	29.3	1.72°	184.04°	315.52	24.17	359.90	145.50	4.71	849.80
14	9-17-2016	29.3	1.02°	184.62°	297.06	26.98	359.90	145.50	4.71	834.16
15	9-18-2016	29.3	0.33°	185.21°	280.05	27.94	372.02	148.97	4.71	833.69
16	9-19-2016	29.3	0.11°	186.03°	265.07	30.84	379.31	151.37	4.71	831.30
17	9-20-2016	29.3	-0.12°	186.82°	248.63	32.13	390.75	155.06	4.71	831.30
18	9-21-2016	29.3	-0.59°	187.48°	231.35	38.89	400.64	158.59	4.71	834.18
19	9-22-2016	29.3	-1.41°	187.82°	201.43	36.83	432.48	169.02	4.71	844.49
20	9-23-2016	29.3	-1.82°	188.48°	184.43	48.45	438.99	172.07	4.71	848.64
21	9-24-2016	29.3	-2.69°	188.83°	156.13	50.55	474.64	184.34	4.71	870.38
22	9-25-2016	29.3	-2.14°	189.96°	141.92	55.97	479.49	186.98	4.71	869.06
23	9-26-2016	29.3	-3.07°	190.39°	118.14	59.25	501.52	195.52	4.71	879.14
24	9-27-2016	29.3	-2.75°	191.25°	93.83	68.76	523.07	203.75	4.71	894.13
25	9-28-2016	29.3	-2.46°	192.12°	64.93	71.33	552.13	214.68	4.71	907.79
26	9-29-2016	29.3	-2.81°	192.71°	36.32	78.40	578.98	225.12	4.71	923.54
27	9-30-2016	29.3	-5.82°	192.16°	184.44	19.35	486.67	188.19	4.78	883.43
28	10-1-2016	29.3	-4.11°	193.11°	232.00	34.49	431.40	168.62	4.71	871.22
29	10-2-2016	29.3	-2.94°	194.92°	263.39	44.92	408.56	161.11	4.71	882.70
30	10-3-2016	29.3	-3.72°	195.64°	264.57	53.69	406.64	161.16	4.71	890.77
31	10-4-2016	29.3	-4.39°	196.31°	291.09	46.75	399.41	158.37	4.71	900.34
32	10-5-2016	29.3	-2.55°	198.04°	319.11	47.10	392.45	156.07	4.71	919.44
33	10-6-2016	29.3	-4.28°	198.16°	321.45	53.17	407.12	160.65	4.71	947.11
34	10-7-2016	29.3	-2.58°	199.93°	369.32	50.39	381.33	152.63	4.71	958.37
35	10-8-2016	29.3	-5.95°	199.46°	379.43	52.71	380.39	152.43	4.71	969.66
36	10-9-2016	29.3	-6.81°	200.11°	413.02	56.78	369.60	149.38	4.71	993.50
37	10-10-2016	29.3	-7.65°	200.77°	443.61	73.92	359.41	146.79	4.71	1028.44
38	10-11-2016	29.3	-8.66°	201.16°	433.26	55.99	392.48	156.03	4.71	1042.48
39	10-12-2016	29.3	-8.38°	202.17°	474.65	49.84	374.49	150.90	4.71	1054.60

5.2. Backup Launch Window

The variation in C_3 across the backup launch window is presented in Figure 9, and the variation in DLA is presented in Figure 10. All of the DLA values for the backup launch window exceed 28.5° (reaching nearly 36° at the beginning of the launch window) and this could lead to reduced performance for launch vehicles launching from the Kennedy Space Center (KSC). However, the C_3 values for the backup launch window are all less, by at least a small amount, than the constant 29.3 km^2/s^2 of the primary launch window. The net impact of those factors on the amount of mass that a given launch vehicle can inject into the Earth departure hyperbola cannot be precisely known until a specific launch vehicle is selected and analyzed with appropriate inputs from the launch vehicle provider. However, the optimization strategy will maintain a constant launch vehicle payload by adjusting C_3 to provide 1955 kg of spacecraft wet mass for the desired DLA value for each date of the backup launch period.

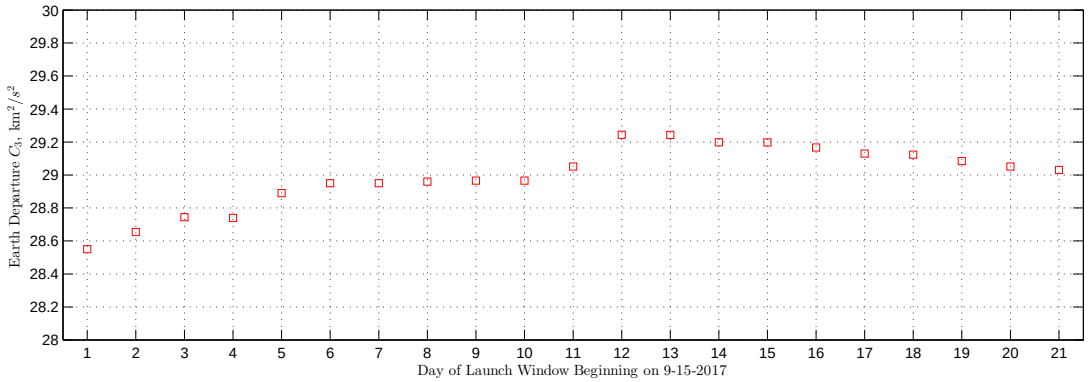

Figure 9: C_3 variation throughout the backup launch window.

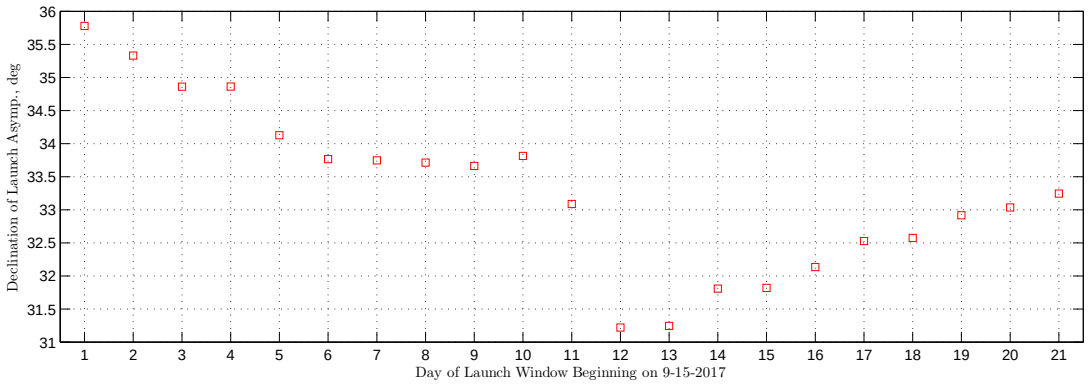

Figure 10: DLA variation throughout the backup launch window.

The total post-launch Δv (for outbound cruise) for each day in the backup launch window is shown in Figure 11. The Δv reaches a minimum of 669.6 m/s on day 11 of the launch window after steadily decreasing to that point from the beginning of the launch window and rising steadily thereafter to the highest overall value of 1123.43 m/s.

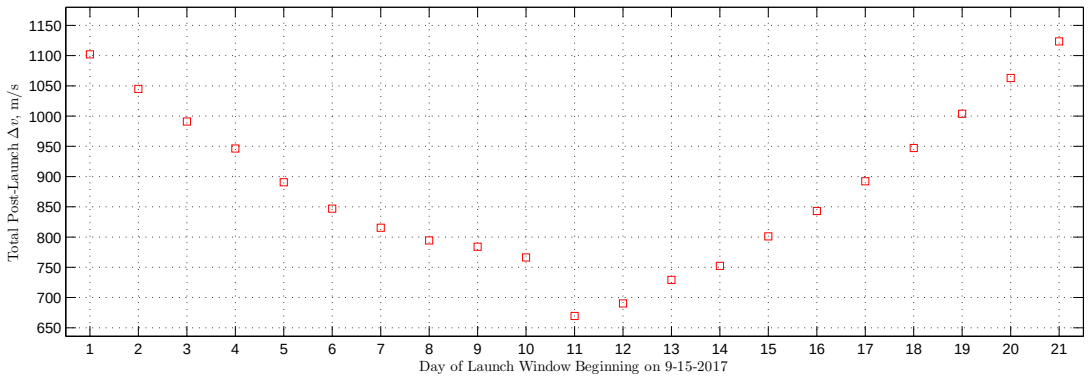

Figure 11: Total Post-Launch Δv variation throughout the backup launch window.

The details of the optimal solutions for each day in the backup launch window are provided in Table 5, including the RLA values and the magnitudes of each individual maneuver. All of the maneuvers except AAM3 vary throughout the launch window in different ways, but the net result is a steady decrease in total Δv until day 11 and a general increase thereafter through day 21. Note that the highest Δv value in the backup launch window (1123.43m/s) exceeds the highest Δv in the primary launch window (1057.57 m/s) and from that perspective additional Δv margin is available if the mission launches during the primary launch window. However, for completeness, if we consider only individual days within the launch window, it is noteworthy that the overall minimum

Δv in the backup launch window (669.6 m/s) is actually less than the minimum Δv available in the primary launch window (831.3 m/s).

Table 5: Optimized outbound cruise trajectory solutions for each day of the backup launch window.

Day	Date	C_3 (km^2/s^2)	DLA	RLA	DSM1 (m/s)	AAM1 (m/s)	AAM2 (m/s)	AAM3 (m/s)	Total Δv (m/s)
1	9-15-2017	28.5	35.78°	185.63°	684.67	288.29	124.42	4.77	1102.15
2	9-16-2017	28.7	35.33°	186.17°	621.44	292.94	126.03	4.70	1045.10
3	9-17-2017	28.7	34.86°	186.76°	562.92	296.10	127.21	4.70	990.93
4	9-18-2017	28.7	34.86°	186.80°	482.37	323.28	136.09	4.70	946.44
5	9-19-2017	28.9	34.13°	187.53°	436.46	315.63	133.74	4.70	890.53
6	9-20-2017	29.0	33.76°	187.90°	374.00	329.66	138.56	4.70	846.91
7	9-21-2017	28.9	33.75°	187.92°	289.71	368.72	152.25	4.70	815.37
8	9-22-2017	29.0	33.71°	187.97°	209.25	412.39	168.11	4.70	794.45
9	9-23-2017	29.0	33.66°	188.03°	134.48	459.35	185.57	4.70	784.10
10	9-24-2017	29.0	33.81°	188.88°	85.04	482.20	194.26	4.70	766.20
11	9-25-2017	29.1	33.09°	189.26°	39.73	444.37	180.80	4.70	669.60
12	9-26-2017	29.2	31.22°	189.28°	59.29	444.38	181.88	4.70	690.25
13	9-27-2017	29.2	31.24°	190.27°	101.60	441.47	181.52	4.70	729.28
14	9-28-2017	29.2	31.81°	191.56°	157.39	417.00	173.27	4.70	752.36
15	9-29-2017	29.2	31.82°	192.49°	206.40	416.42	173.58	4.70	801.10
16	9-30-2017	29.2	32.13°	193.58°	263.01	405.42	170.06	4.70	843.19
17	10-1-2017	29.1	32.53°	194.70°	321.22	398.45	167.91	4.70	892.28
18	10-2-2017	29.1	32.57°	195.63°	378.31	396.52	167.70	4.70	947.22
19	10-3-2017	29.1	32.92°	196.70°	437.79	394.26	167.07	4.70	1003.83
20	10-4-2017	29.1	33.03°	197.64°	495.71	394.89	167.65	4.70	1062.94
21	10-5-2017	29.0	33.25°	198.63°	561.13	391.36	166.24	4.70	1123.43

6. Conclusions

In this paper we have provided an overview of the OSIRIS-REx mission design with an emphasis on the interplanetary trajectories to rendezvous with the asteroid and then return to Earth with the regolith sample for entry, descent, and landing. OSIRIS-REx has robust primary and backup launch windows that leave the spacecraft with Δv even on the worst day of the launch window and with other contingencies and redundancies built into the Δv budget.

We have shown the benefits of the advanced OSIRIS-REx trajectory design that includes optimized Deep Space Maneuvers (DSMs), multiple revolutions about the Sun, and an Earth Gravity Assist (EGA) to achieve very affordable mission Δv costs by trading time at the asteroid for reduced Δv. We also describe how this trade is made possible by designing the mission to span approximately one Earth/asteroid synodic period.

The destination for the OSIRIS-REx mission, potentially hazardous near-Earth asteroid (101955) 1999 RQ_{36}, is an exciting science target and our interactions with it will provide crucial knowledge for future missions to asteroids for robotic and human exploration, scientific understanding, and defending our planet against asteroid impacts.

Acknowledgments

This work is supported by the OSIRIS-REx Asteroid Sample Return Mission project, for which Dr. Dante Lauretta is the Principal Investigator, within NASA's New Frontiers Program. The authors are grateful for contributions to this work by the OSIRIS-REx Flight Dynamics team and other OSIRIS-REx subsystem teams. The authors are also appreciative of support and technical input from the OSIRIS-REx Science team liaisons to the Flight Dynamics team, Dr. Steven Chesley and Dr. Daniel Scheeres.

References

[1] Russell, J., Mink, R., Boynton, W., Lauretta, D., Beshore, Ed., Sutter, and B., Bierhaus, B., OSIRIS-REx Techniques Applied to Earth-Crossing Object Deflection, in: Proceedings of the IAA Planetary Defense Conference 2013, Flagstaff, AZ. April 15-19, 2013.

[2] Berry, K., Sutter, B., May, A., Williams, K., Barbee, B. W., Beckman, M., Williams, B., OSIRIS-REx Touch-And-Go (TAG) Mission Design and Analysis, in: Proceedings of the 36th Annual AAS Guidance and Control Conference, AAS/AIAA Paper AAS 13-095, Breckenridge, CO. February 1-6, 2013.